

RESEARCH PAPER



***IRX1* hypermethylation promotes heart failure by inhibiting CXCL14 expression**

Longhuan Zeng, Nanyuan Gu, Jiayi Chen, Guangyong Jin, and Yongke Zheng

Department of Intensive Care Unit, Affiliated Hangzhou First People's Hospital, Zhejiang University School of Medicine, No. 261 Huansha Road, Hangzhou, 310006, China

ABSTRACT

To identify the mechanism and functions of *IRX1* in heart failure (HF) and provide evidence for new therapies. Bioinformatic analysis was performed to select target genes in HF cells compared to normal groups. Experimental rats were treated in a controllable manner to explore how *IRX1* methylation accounted for this disease *in vivo*. Cardiac ultrasonic and morphologic examinations were conducted to test the mouse heart and evaluate the degree of cardiac impairment at in the level of organization. GSEA analysis revealed the relative enrichment of functions. Immunofluorescent assays, western blotting and qRT-PCR were used to determine the DNA methylation and expression levels. *IRX1* was hypermethylated in heart failure and identified as a target gene by bioinformatic analysis. Transverse aortic constriction (TAC) induced heart failure in rats, while 5-aza-2'-deoxycytidine (5-Aza) alleviated heart failure in rats according to medical cardiac indexes. Western blotting and qRT-PCR revealed that a conspicuous difference in the expression of *IRX1* and *CXCL14* between HF and normal cardiac cells. As a result of gene methylation, left ventricular hypertrophy and cardiac fibrosis is usually accompanied by heart failure. Moreover, the results implied that the demethylation of *IRX1* improves heart failure *in vivo* and *in vitro*. *IRX1* methylation induced damaged cardiac function and even heart failure, which has important implications for HF treatment and diagnosis.

ARTICLE HISTORY

Received 13 February 2019
Revised 17 September 2019
Accepted 24 September 2019

KEYWORDS

DNA methylation; heart failure; 5-aza-2'-deoxycytidine

Introduction

Cardiovascular diseases (CVD) represent considerable morbidity and mortality, of which heart failure is often observed as the end stage [1]. Heart failure, as a growing health concern, affects over 20% of persons and contributes to 11% of deaths worldwide [2]. Clinical medicine diagnoses heart failure as a complex syndrome accompanied by reduced cardiac output, insufficient blood supply and increased risk of cardiac arrest [3]. As fetal genes, atrial natriuretic peptide (ANP) and brain natriuretic peptide (BNP) have been confirmed to correlate well with the clinical severity and prognosis of this disease [4]. Despite tremendous scientific efforts during the past several decades, heart failure remains high-risk and fatal, with an incidence that is expected to increase.

Specialists classify the current treatments for heart failure into five categories: drug treatment [5], auxiliary device, heart transplantation, cell transplantation and gene therapy, among which medicine is the most widely used [6]. Most drugs primarily target neuroendocrine mechanisms, including angiotensin-converting enzyme (ACE) inhibitors, angiotension

receptor type 1 (AT1) antagonists, b-adrenoceptor antagonists (BAA), aldosterone receptor antagonists, diuretics and digoxin [7]. Given that evolving therapeutic strategies fail to generate a satisfactory declining prevalence of HF, new molecular targets are urgently needed.

The development and progression of heart failure cannot be separated from epigenetic changes [8]. Unlike genetic alterations, the potential reversibility and heritability of chromosomal component modifications make epigenetic mechanisms attractive and promising targets for therapeutic intervention [9]. Epigenetic mechanisms, such as microRNA and DNA methylation, have been implicated in the aberrant gene expression observed heart failure in previous studies [10]. Moreover, several studies have shown that DNA methylation can silence or activate expression patterns of genes that drive the CVD process, including left ventricular hypertrophy (LVH) and myocardial fibrosis (MFS) [11]. However, the detailed mechanism and potential clinical application of DNA methylation in HF needs further analysis.

Iroquois homeobox 1 (*IRX1*), a transcription factor, plays a crucial role in embryonic development. Recently, *IRX1* has emerged as a potential suppressor gene in rheumatoid arthritis (RA), congenital heart disease (CHD) and tumors, such as gastric cancer (GC) and osteosarcoma [12–14]. Changlong Guo *et al.* linked an aberrant non synonymous mutation in *IRX1* to irregular cardiac function and *IRX1* hypermethylation has been frequently detected in HF cell lines [13]. These findings suggest that *IRX1* likely plays a role in the precise molecular mechanisms of heart failure. In addition, the association of *IRX1* methylation with myocardial function in HF patients is of interest.

Chemokines are a superfamily of small chemotactic cytokines, Chemokine (C-X-C motif) ligand 14 (*CXCL14*) is a member of the *BRAK* superfamily [15]. Previous studies have reported the CXC chemokine superfamily plays an important role in inflammatory, autoimmune and tumorigenic functions [16,17]. Normal human epithelial cells constitutively express *CXCL14*, its expression is frequently reduced in cervical, prostate, and oral cancers [18,19]. Consistently, many studies have reported that *CXCL14* was highly expressed in normal tissues, especially in normal kidney tissues, but absent in the tumor cell lines and primary tumors [18,20]. *CXCL14* is generally considered a tumor suppressor [21,22], but several recent studies have reported the opposite results. For example, the upregulation of *CXCL14* in pancreatic cancer promotes the invasion of tumor cells [23].

Furthermore, *IRX1* and *CXCL14* may have interactive effects on cardiac function and hence provide a new approach to heart failure.

In our study, *IRX1* was epigenetically activated in HF samples and its expression was negatively associated with promoter hypermethylation. In addition, the downregulation of *IRX1* resulted in decreased *CXCL14* expression levels. More importantly, this study is a significant step forward in ascertaining a potential target for epigenetic-based heart failure therapy.

Methods

Bioinformatic analysis

Here, the ChIP Analysis Methylation Pipeline (ChAMP) package, differential analysis of limma

package, and gene set enrichment analysis (GSEA) were applied to show significant differences between two biological states based on the NCBI GEO DataSets database (GSE54681, <https://www.ncbi.nlm.nih.gov/geo/>). We identified the differential gene expression between HF and normal tissues by comparing the reads of each sample to the genome according to screening conditions ($|\text{fold change}| > 2$ and P value < 0.05). Upregulated signal pathways were predicted and analyzed by GSEA, and then related to differentially expressed genes [24].

Animal preparation

Male six-month-old Sprague–Dawley rats (225 to 250 g) were purchased from the Chinese Academy of Sciences of Shanghai. Animal experiments were approved by the Animal Care and Use Committee and were performed according to the official recommendations of the National Institutes of Health guidelines and the Affiliated Hangzhou First People's Hospital, Zhejiang University School of Medicine.

TAC surgery

Six-week-old rats underwent the TAC operation. All animals were anesthetized with 2.0% inhalational isoflurane, and the aortic arch was tied with a 4/0 silk suture between the brachiocephalic and left common artery with an overlaying 20-gauge needle. After ligation, the needle was quickly removed, and the skin was closed. The sham operation was identical, except that the thread was not ligated [25,26]. We randomly divided twenty rats into 4 groups: (i) Sham control, (ii) TAC, (iii) Sham+5-Aza, (iv) TAC+5-Aza. Rat heart failure was induced by TAC for 4 weeks. 5-Aza was administered intraperitoneally during the last 2 weeks.

Echocardiography

Echocardiography was performed using the VIVO 2100 system (Visual Sonics, Canada) to evaluate cardiac function. During the procedure, the animals were under inhaled anesthesia (isoflurane 2%), and body temperature was maintained using a heat mat. The cine loops were analyzed for left

ventricular developed pressure (LVDP), ejection fraction (EF) and maximal rate of the increase in left ventricular pressure (dp/dt max).

Histological analysis

Whole hearts were fixed with 10% formalin, embedded in paraffin, and sectioned at 7- μ m intervals. Each slide had 10 sections, which started at the apex and ended at the suture ligation site (approximately 50 slides). Every 4th slide was stained with picosirius red staining to identify areas of fibrosis [27]. Hematoxylin and eosin staining was performed by Rapid Chrome hematoxylin and eosin staining kit (Thermo Scientific, USA) according to the manufacturer's instructions [28].

Measures of apoptosis

A TUNEL Apoptosis Detection Kit (FITC) (YEASEN, China) was used to label apoptotic bodies according to the manufacturer's guidelines. The TUNEL positive cells in the stained images were counted to indicate the apoptotic rate [27].

Isolation of cardiac myocytes

The rats were adequately anaesthetized with 75 mg/kg ketamine and 5 mg/kg xylazine injected intramuscularly, and the respiration rate of the rats was closely monitored to determine the degree of anesthesia. Then, the hearts were removed and maintained in a suitable environment. Cardiomyocytes were obtained by Langendorff perfusion with 0.25 mg/mL Liberase enzyme solution (DH Research Grade, Roche, and Basel, Switzerland). Then cardiac myocytes were plated (1 \times penicillin, streptomycin, glutamine, 10% horse serum, 5% newborn calf serum, 1.68% M199 salts in DMEM) for 24 h and transferred to DMEM containing 0.1% insulin/transferrin/sodium selenite supplement [29].

Global DNA methylation measurement

Genomic DNA was isolated from left ventricles and incubated with a mixture of phosphodiesterase I, benzonase nuclease, and shrimp alkaline phosphatase. HPLC coupled with tandem mass

spectrometry (HPLC-MS, SHIMADZU) was detected to quantify methyl-cytosine (Cm) and cytosine (C) in multiple reaction monitoring mode. The results are represented as the Cm/C ratio [11].

Western blotting

We resolved proteins on 10% SDS-PAGE gels followed by transfer to PVDF membranes (Millipore). Subsequently, the proteins bands were detected according to standard lab protocols. The membranes were incubated with Anti-IRX1 antibody (ab98343, Abcam), Anti-CXCL14 antibody (ab36622, Abcam), Anti-GAPDH antibody (ab181602, Abcam) [30].

qRT-PCR

Transcript levels were determined by RT-PCR using a QuantiTect SYBR Green real-time PCR Kit (11,746,500, Invitrogen). Total RNA was extracted from samples with Trizol reagent (A33252, Invitrogen) following the manufacturer's instructions. Reverse transcription was performed at 50°C for 20 min, and the cDNA was amplified in 20 μ l reaction volumes using 10 pmol of primers for 37 cycles at 94°C for 10 s, 57°C for 15 s, and 72°C for 5 s. Notably, GAPDH acted as an internal control to calculate the relative abundance of the mRNAs [31]. The primer sequences are listed in Table 1.

Quantitative methylation-specific PCR

DNA collected from samples was treated with sodium bisulfite at 55 °C for 16 hours. Bisulfite-treated DNA was used as a template for real-time fluorogenic methylation-specific PCR (MSP) using primers created to amplify promoter binding sites containing possible methylation sites based on MethPrimer [32] and listed in Table 1.

Gene ontology (GO) annotation analysis

For the GO functional annotation analysis of the genes targeted by *IRX1* and differentially expressed genes, we applied the R package Metascape (<http://metascape.org/gp/index.html#/main/step1>). The

Table 1. Primers used in this study.

Gene		Sequence (5'-3')
<i>IRX1</i>	Forward	GAAATCTGGGCACAGTCCA
	Reverse	CACAGTGGTTTTGCTCGGTG
<i>CXCL14</i>	Forward	GCAGGGCAATTGGGAACAAG
	Reverse	GGGTGCAGGGTCATCCTAAC
<i>ANP</i>	Forward	CCGGTACCGAAGATAACAGC
	Reverse	CCGGTACCGAAGATAACAGC
<i>BNP</i>	Forward	CTGGGAAGTCTAGCCAGTCTCCA
	Reverse	GCGACTGACTGCGCCGATCCGGT
<i>α-MHC</i>	Forward	ACAGAGTGCTTCGTGCCTGAT
	Reverse	CGAATTCGAGGGTCTCTGC
<i>β-MHC</i>	Forward	GCTACCCAACCCTAAGGATGC
	Reverse	TCTGCCTAAGGTGCTGTTC
<i>GAPDH</i>	Forward	AACGACCCCTCATTGACCT
	Reverse	CCCCATTTGATGTTAGCGGG
<i>MSP(M)</i>	Forward	TTTTTTAAGAGTAAGGGGGTTAGC
	Reverse	TAAAATATTCAATAAATCAACGCT
<i>MSP(UM)</i>	Forward	TTTTTAAGAGTAAGGGGGTTAGTGA
	Reverse	TAAAATATTCAAATAAATCAACACT
<i>shIRX1-A</i>	Forward	CACCGCTGCTTATTATCCCTATGG
	Reverse	CGAACCATAGGGATAATAAGCAGGC
<i>shIRX1-B</i>	Forward	AAAAGCCTGCTTATTATCCCTATGG
	Reverse	TTCGCCATAGGGATAATAAGCAGGC
	Forward	CACCGGAGAGCATTGACATCGATCA
	Reverse	CGAATGATCGATGCAATGCTCTCC
		AAAAGGAGAGCATTGACATCGATCA
		TTCGTGATCGATGCAATGCTCTCC

M: methylation primer; UM: unmethylation primer.

R package Go plot was used for analysis visualization. The protein-protein interaction (PPI) network and the cluster of differentially expressed genes were drawn using Cytoscape software (version: 3.3.0).

Microarray

All sample labeling and microarray chip processing were performed at the Veterans Medical Research Foundation Microarray & NGS Core in San Diego. RNA integrity was also validated by the ratio of 28S/18S ribosomal RNA using an Agilent 2100 Bioanalyzer. cDNA was synthesized from 1 μ g of total RNA (pooled 500 ng from each rat) using an Affymetrix GeneChip WT PLUS Reagent Kit. Whole transcriptome microarray analysis was performed using the GeneChip Rat Gene 2.0 ST array (Affymetrix). Colocalization was measured using in-house software to measure distances between clusters [33].

Immunohistochemical staining

Frozen sections of rat cardiac tissues were stained with anti-*IRX1* antibody (ab180860, Abcam),

DAPI (Beyotime) and WGA (Invitrogen). Immunofluorescence images showed the membranes (green) [12].

Statistical analysis

Graph Prism 6.0 software (GraphPad Prism, San Diego, CA) was used for data analysis and diagram generation. Values are shown as the mean \pm standard deviation (SD). Depending on the situation, the differences among groups were evaluated by one-way analysis of variance (ANOVA) or two-tailed Student's t-test. All data were derived from at least three repetitions for each type of experiment. The data group with a *P*-value < 0.05 was regarded as a significantly different group [34].

Results

The CpG sites methylated abnormally in HF compared to normal groups

Multi-dimensional scaling (MDS) identified 1000 variable positions, revealing significant differences between HF and normal tissues (Figure S1(a)). Different beta value distributions were displayed by Type-I and Type-II assays and normalization procedures were used to adjust differences between probe types, in which 0 represented unmethylated sites while 1 represented fully methylated sites (Figure S1(b)). Figure S1C shows the comparison of the beta value density plots from each sample and identified the poor performing arrays basing on a large deviation from the rest of the samples. The dendrogram for 481,173 probes intuitively displayed a clear distinction between normal and HF tissues (Figure S1(d)). For a heatmap of 1000 variable CpGs revealed hypermethylation in HF tissues and hypomethylation in normal groups (Figure S1(e)).

IRX1 and its relevant pathway were identified

As the heatmap of the top 20 differently methylated genes exhibited, several genes (*CHL1*, *PTRF*, *SOX1* and *GREB1L*) were less methylated in normal tissues than in HF tissues (Figure 1(a)) and *IRX1* was selected as the target gene. Upregulated pathways in normal and HF tissues were explored (Figure 1(b)) and the position in the ranked list of genes according to GSEA

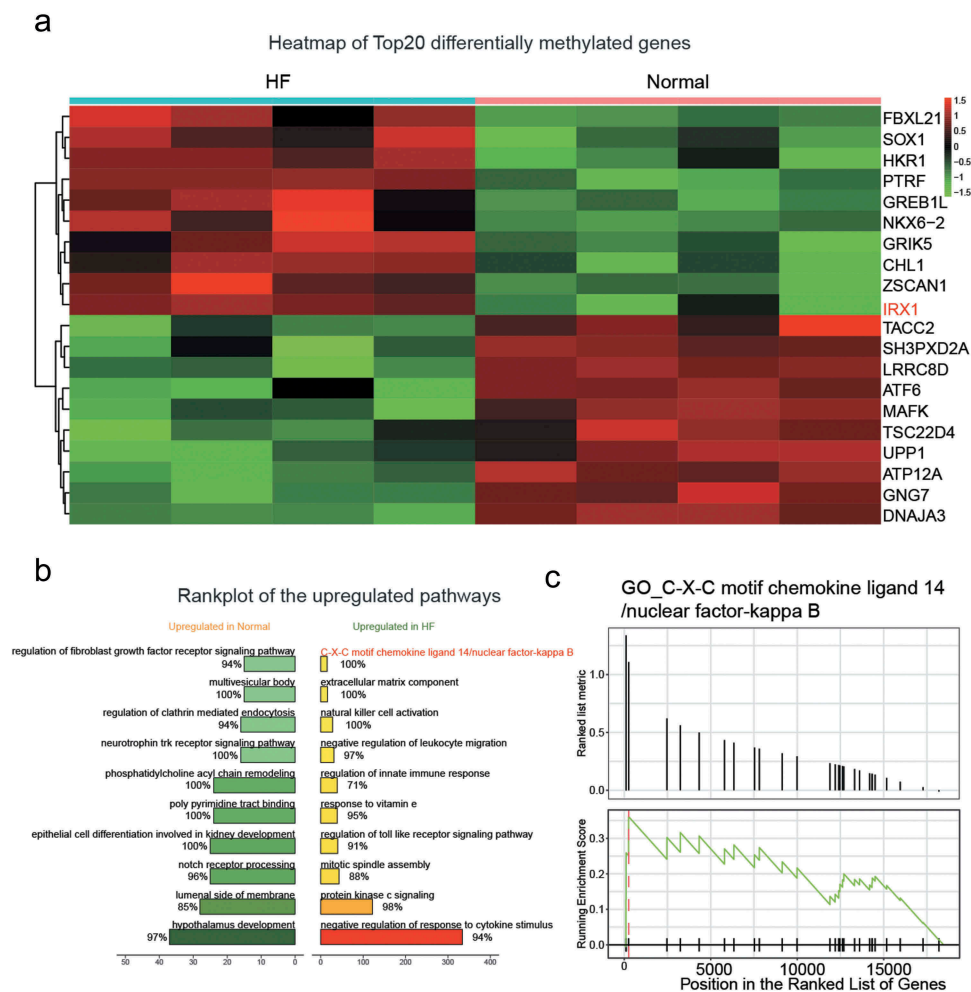


Figure 1. Heatmap of the methylation level and target pathway in HF and normal pairs.

(a) The heatmap of the top 20 DEGs. *IRX1* showed a higher level of methylation in HF than normal. HF: heart failure; DEGs: differentially expressed genes. (b) Rank plot of the upregulated pathway in normal and HF. (c) C-X-C motif chemokine ligand 14/nuclear factor-kappa B (NF- κ B) was identified through GO.

analysis (Figure 1(c)) indicated a significant correlation between *IRX1* expression and C-X-C motif chemokine ligand 14/nuclear factor-kappa B.

5-Aza-2'-deoxycytidine suppressed *IRX1* hypermethylation and restored gene expression in heart failure rats

Echocardiography by direct LV catheterization assessed the cardiac function in experimental rats (Figure 2(a-f)). Pathological hypertrophy was triggered over a 4-week period through an ascending TAC-induced pressure overload, producing a growth in the left ventricle to body weight ratio, while dramatically decreases in left ventricular

development pressure (LVDP), dp/dt_{max} (Figure 2(a-c)) and ejection fraction (Figure 2(e-f)). Strikingly, the rats received a complete reversal of TAC-induced heart injuries due to treatment with 5-Aza (Figure 2(a-c,e,f)). Additionally, hematoxylin and eosin staining showed that TAC had disordered arrangement of cardiomyocytes, which was alleviated by 5-Aza treatment (Figure 2(d)). These predictable differences showed representative symptoms of heart failure.

TAC-induced heart failure enhanced global genomic DNA methylation (Figure 3(a)) and a gene-specific *IRX1* methylation (Figure 3(b)). Significant increases in the mRNA expression of genes the ANP and BNP genes in the left ventricle

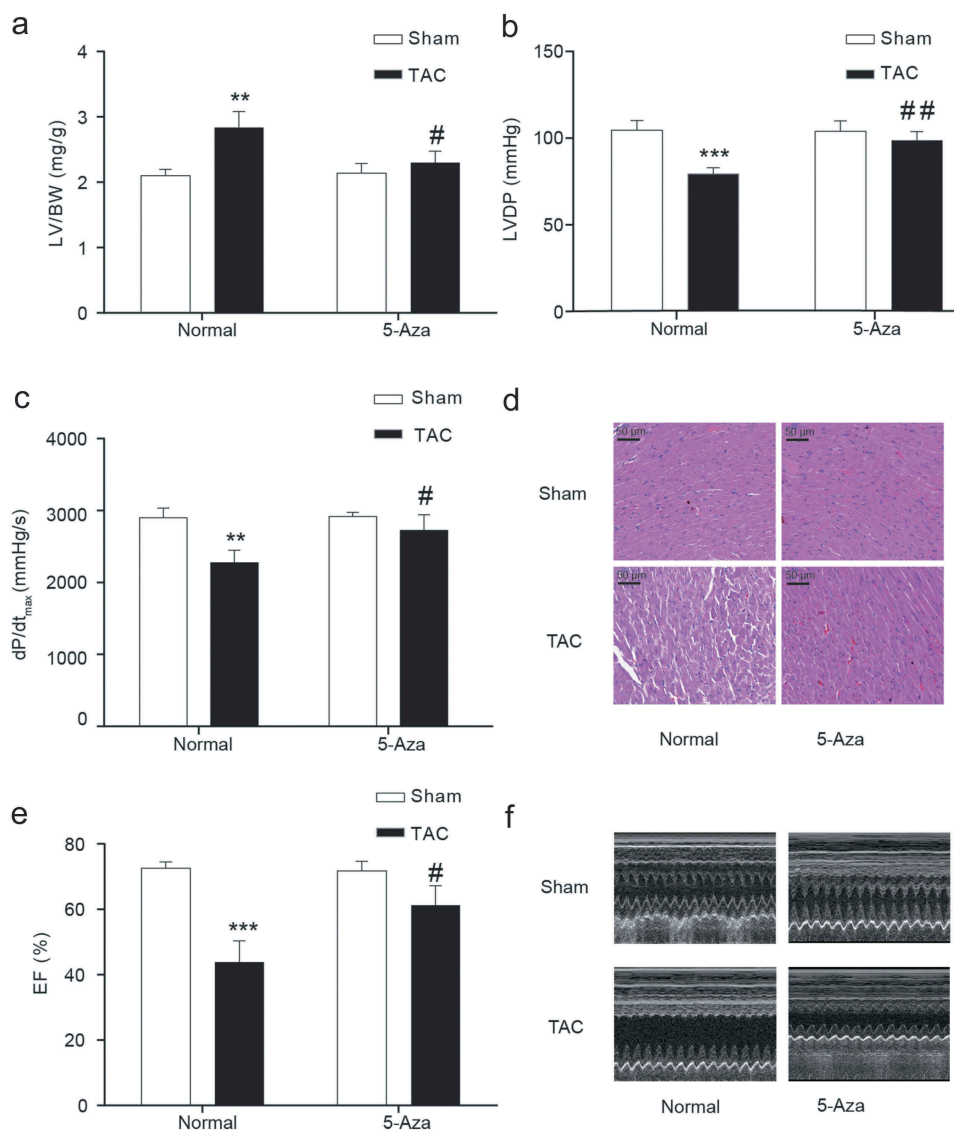


Figure 2. Cardiac functions of rats in each group.

(a) LV/BW (b) LVDP (c) The maximal rate of the increase in left ventricular pressure (dp/dt max) (d) HE staining of cardiac tissue. (E-F) Ejection fraction (%) measured by echocardiography. LV, left ventricle; BW, body weight, EF, ejection fraction. Data are presented as the mean \pm SD of five animals; ** $P < 0.01$, *** $P < 0.001$ vs. Sham-Normal group, # $P < 0.05$, ## $P < 0.01$ vs. TAC-Normal group.

symbolize the occurrence of heart failure (Figure 3 (c,d)), Additionally, 5-aza-2'-deoxycytidine treatment reversed the expression of α -MHC and β -MHC, two markers of pathological cardiac hypertrophy (Figure 3(e,f)). Moreover, the abundant *IRX1* mRNA (Figure 4(a)) and protein (Figure 4 (b)) inhibition were observed with heart failure. However, the treatment of rats with 5-aza-2'-deoxycytidine reversed the low-expression of *IRX1* induced by TAC and normalized to the Sham group (Figure 4(a-c)). That is, epigenetic changes such as DNA methylation are always reversible in diseases.

5-aza-2'-deoxycytidine protected tac-induced myocardial fibrosis and apoptosis by upregulating CXCL14 expression

To investigate whether 5-aza-2'-deoxycytidine protected cardiac function by reducing myocardial fibrosis and myocardial apoptosis, we detected the fibrotic area and myocardial apoptosis after 2 weeks of 5-Aza treatment. *IRX1* hypomethylation facilitated maladaptive cardiac remodeling because 5-Aza-2'-deoxycytidine significantly abrogated fibrotic (Figure 4(d,f)) and apoptotic (Figure 4(e,g)) responses to TAC-induced heart failure.

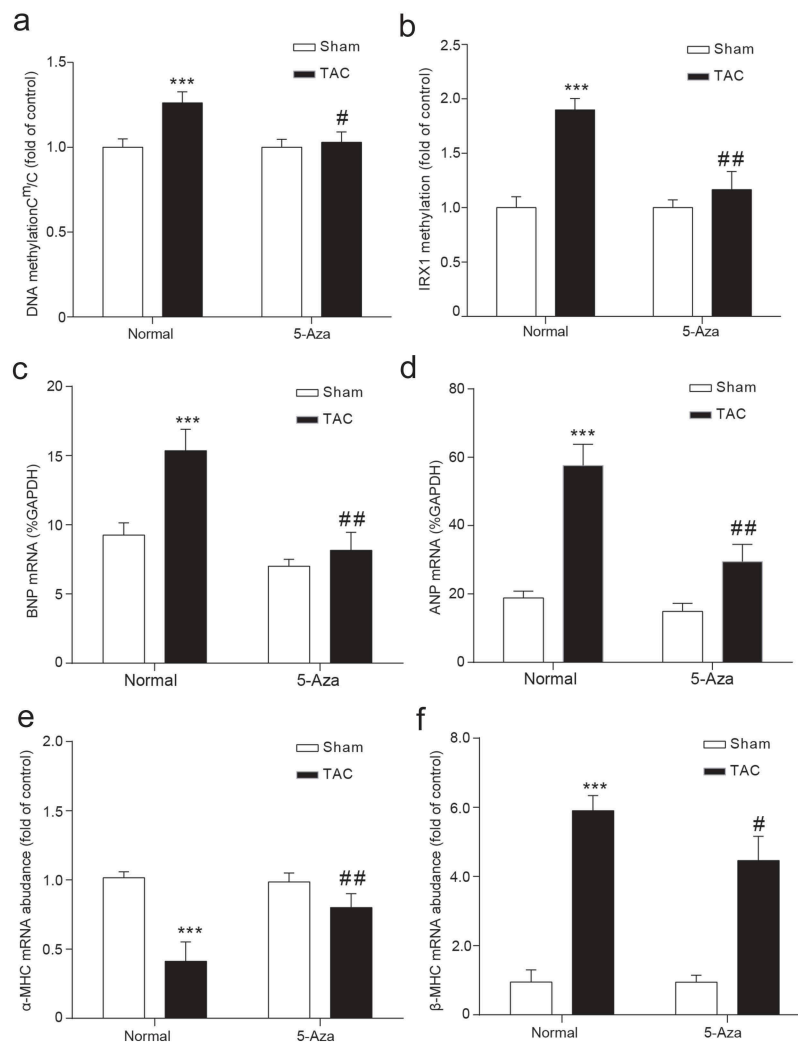


Figure 3. Differential gene expression and methylation in HF rats.

(a-b) ANP and BNP are significant symbols of HF. (c) Cm/C in LV. (d) IRX1 methylation was determined by MSP. (e) α -MHC mRNA expression. (f) β -MHC mRNA expression. Data are presented as the mean \pm SD of five animals; *** P < 0.001 vs. Sham-Normal group, # P < 0.05, ## P < 0.01 vs. TAC-Normal group.

To probe the relationship between *IRX1* and *CXCL14*, qRT-PCR and western blotting were used to determine the mRNA and protein expression of *CXCL14* (Figure 5(a,b)). To further reveal the relationship between *IRX1* and *CXCL14*, we generated 2 lentiviral constructs encoding *IRX1*-targeting shRNAs, and western blot assay confirmed that the ShIRX1 lentiviral construct could inhibit the protein expression level of IRX1, and the over expression lentiviral could increase the protein expression level of IRX1 (Figure 5(c-d)). The lentivirus was transfected into cardiac myocytes, and *CXCL14* mRNA and protein expression were detected. As expected, we found that *IRX1* knockdown reduced the expression of both

CXCL14 mRNA and protein (Figure 5(e,g,h)). We further confirmed the relationship between *IRX1* and *CXCL14* through gain-of-function studies, and found that *CXCL14* mRNA and protein levels were upregulated by IRX1 overexpression (Figure 5(f-h)). According to the experimental results obtained, there is a positive regulatory relationship between *IRX1* and *CXCL14*. Therefore, *IRX1* may activate *CXCL14* expression to protect TAC-induced myocardial fibrosis and apoptosis.

Discussion

In our study, *IRX1* was identified as a hypermethylation-activated gene and the

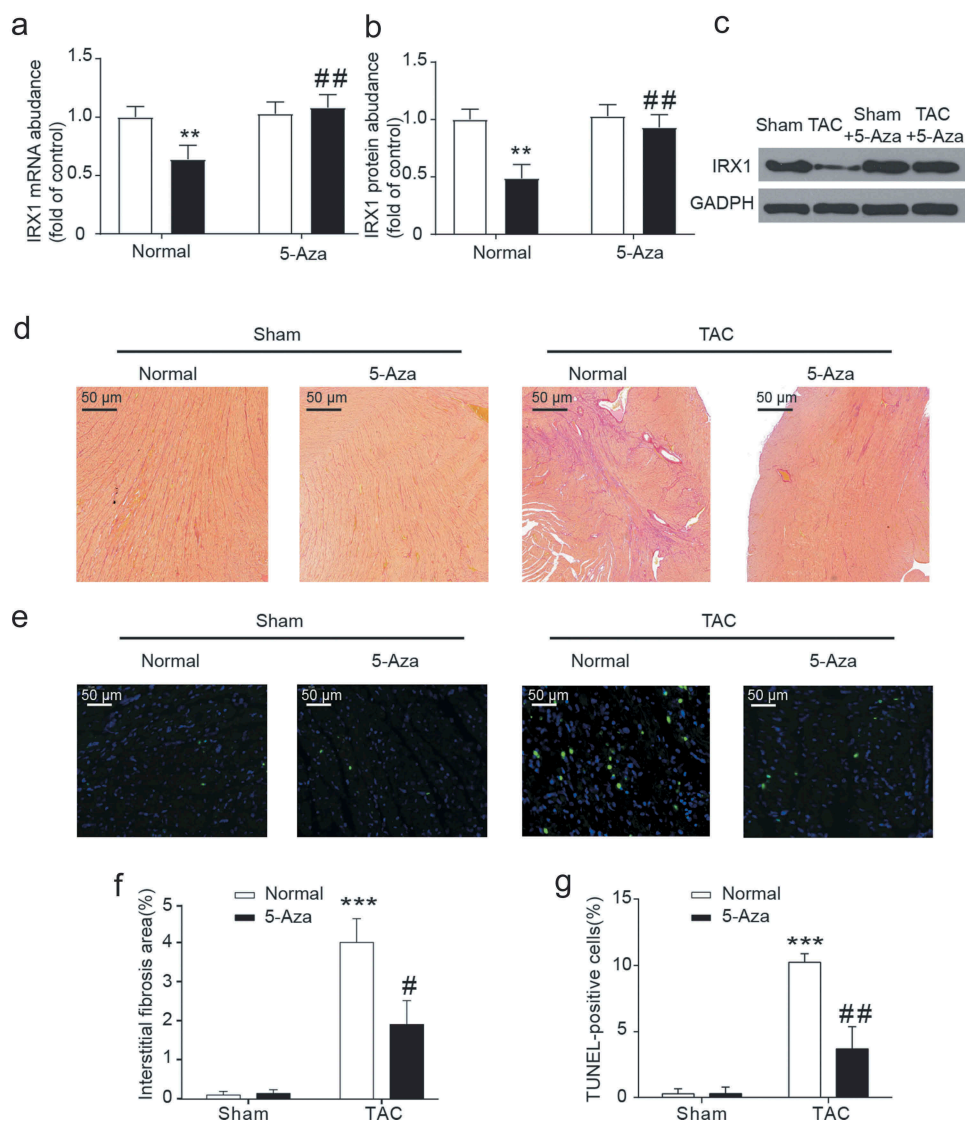


Figure 4. 5-Aza-2'-deoxycytidine reversed cardiac hypertrophy and *IRX1* downregulation in TAC-induced heart failure.

(a) qRT-PCR determined *IRX1* mRNA expression in the left ventricles. (b-c) Western blot analysis determined *IRX1* protein expression in the left ventricles. (d, f) Sirius red staining and morphometric analysis identified interstitial cardiac fibrosis. (e) TdT-mediated dUTP-biotin nick end labeling (TUNEL) staining to perceive detect apoptotic cells. (g) TUNEL positive cells ratio. Data are presented as the mean \pm SD of five animals; ** $P < 0.01$, *** $P < 0.001$, vs. Sham-Normal group, # $P < 0.05$, ## $P < 0.01$ vs. TAC-Normal group.

suppression of *IRX1* decreased *CXCL14* expression levels in rat models of heart failure. Our data show that the 5-Aza-induced hypomethylation of *IRX1* positively regulates adaptation during heart failure. Therefore, we concluded that the therapeutic targeting of the *IRX1* pathway will be a predictable strategy for suppressing heart failure. A large amount of evidence indicates that DNA methylation plays a vital role in the progression of disease initiation and progression due to epigenetic adjustment [35]. To understand its role in regulating gene expression and cell phenotype, high-throughput sequencing or array platforms

focused on the methylation of the promoter CpG islands of genes have enabled the profiling of methylation marks at a genome-wide scale [36]. Recent studies have shown that DNA methylation is altered during cardiomyocyte proliferation or apoptosis and ventricular remodeling [37]. On the other hand, 5-Aza, as a cytidine nucleoside analog, is the most popular demethylation agent that blocks DNA methylation by forming a covalent bond in which DNMTs are removed from the active nuclear pool [38]. Here, the results of bioinformatic analysis showed that the DNA methylation level of genes in HF tissues was

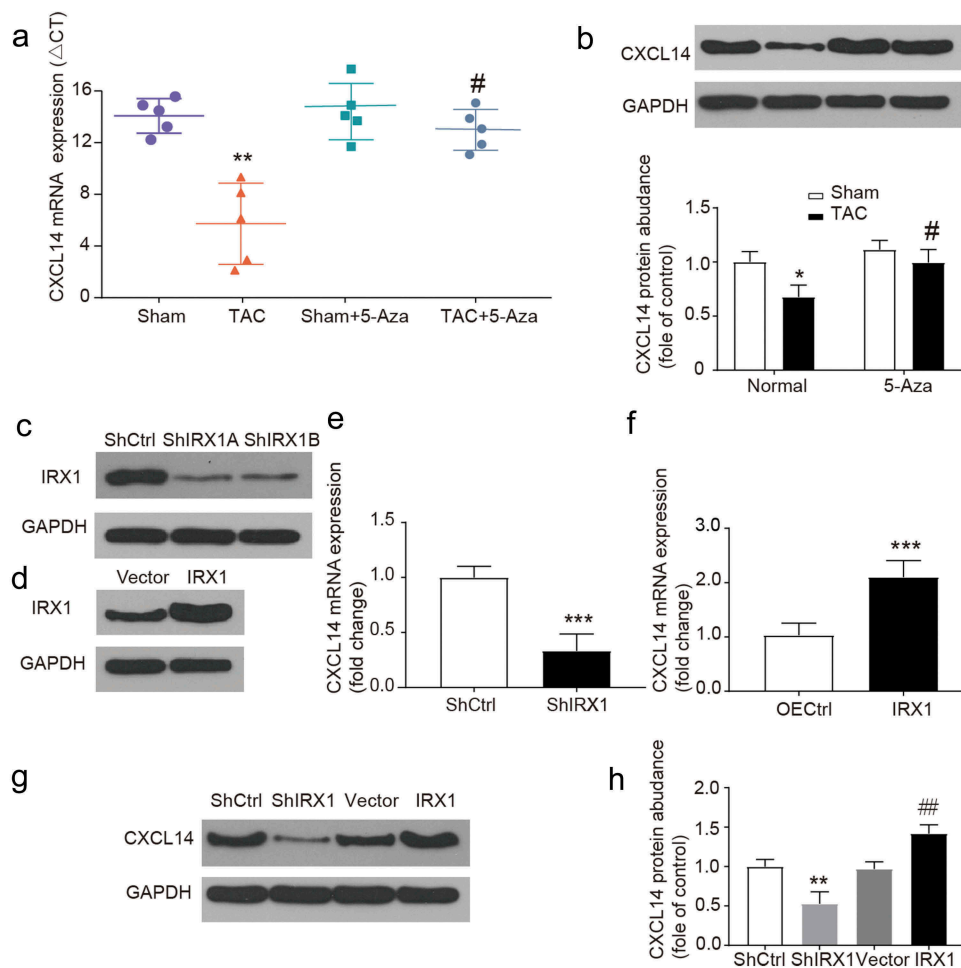


Figure 5. Repression of *CXCL14* gene expression is relevant to *IRX1*.

(A-B) *CXCL14* mRNA and protein expression was downregulated in TAC rats. Data are presented as the mean \pm SD of five animals; $^{**}P < 0.01$, vs. Sham-Normal group, $^{\#}P < 0.05$, vs. TAC-Normal group. (C) The effect of *IRX1*-targeting shRNAs was confirmed by western blot analysis. (D) The efficiency of *IRX1* overexpression was confirmed by Western blot analysis. (E) *CXCL14* mRNA levels were downregulated by *IRX1* shRNA transfection. Data are presented as the mean \pm SD, $^{***}P < 0.001$ (F) *CXCL14* mRNA levels were upregulated by *IRX1* overexpression. Data are presented as the mean \pm SD, $^{***}P < 0.001$ (G-H) *CXCL14* protein levels were downregulated by *IRX1* shRNA transfection and upregulated by *IRX1* over expression. Data are presented as the mean \pm SD, $^{***}P < 0.001$, vs. ShCtrl group, $^{\#\#}P < 0.01$ vs. Vector group.

significantly different from that in normal tissues. In further animal experiments, 5-Aza enhanced *IRX1* expression and inhibited the development of HF, which implied that *IRX1* might become a molecular target of HF.

The Iroquois homeobox family plays multiple roles in drug discovery, disease investigation and cell-based therapies[39]. For example, *IRX3* downregulation in breast cancer was linked to poor clinical outcomes, and interaction between *IRX4* and *IRX5* controls cardiac potassium channel Kv4.2 gene transcription [40,41]. Importantly, variants of the *IRX1* gene were reported to contribute to the increased susceptibility of CHD [13]. Therefore,

treatment strategies that target *IRX1* signaling must consider its various roles to avoid increasing the risk of other diseases [42]. Our study showed that *IRX1* was expressed at a low level in the cardiomyocytes of HF rats and this protein functions as a controlling gene, suggesting that *IRX1* might specifically function in heart development.

Accurately replicating heart failure in animal models is necessary for the exploration of promising disease targets [43]. Decades of experience remind us that clinical advances are usually aroused from relatively simple experimental design of animal models [44]. A recent study documented that echocardiography data could easily be

interpreted by human echocardiographers, suggesting that the molecular imaging of animal hearts are compatible with human technology despite technological limits in some areas [45,46]. In this study, rat models of heart failure were established by TAC induced pressure overload over 4 weeks, with echocardiography to detect cardiac function.

Cardiomyocyte fibrosis is as an important cause of various cardiovascular diseases that develop into heart failure [47]. Notably, understanding the molecular mechanisms of cardiac fibrosis can lead to new approaches for HF prevention or management [48]. Fibroblast growth factors, secreted into the extracellular and interstitial space by cardiac cells, promote and sustain, cardiac fibrosis [49]. Immunohistochemistry staining in the present study showed that myocardial fibrosis was higher in the heart failure group than in the normal group. Our data also indicated that *CXCL14* exerts a synergistic effect with *IRX1* to attenuate myocardial fibrosis and cardiomyocyte apoptosis. Therefore, we proposed that *IRX1* inhibited fibrosis formation, thereby improving cardiac function. This study showed that the reversible regulation of *IRX1* was essential during the development of heart failure. *IRX1* hypermethylation decreased the expression of *CXCL14* and increased fibrosis formation, which dramatically impaired cardiac function. However, the exact regulatory mechanisms for *IRX1* silencing and how *IRX1* and *CXCL14* cooperate in heart failure remain elusive. Nevertheless, these observations will have potential implications for recovery from heart failure in the future.

Disclosure statement

No potential conflict of interest was reported by the authors.

Funding

This work was supported by the Project of Hangzhou Science and Technology (Grant Number: 20180533B97).

Ethics approval and consent to participate

The study protocol conforms to the official recommendations of the National Institutes of Health guidelines and the

Affiliated Hangzhou First People's Hospital, Zhejiang University School of Medicine.

Authors' contributions

Contributing to the conception and design: LH Z, NY G and JY C; Analyzing and interpreting data: LH Z, NY G, GY J and YK Z; Drafting the article: LH Z, JY C and YK Z; Collection of funding: YK Z; Revising it critically for important intellectual content: YK Z; Approving the final version to be published: All authors.

References

- [1] Hwee DT, Kennedy AR, Hartman JJ, et al. The small-molecule fast skeletal troponin activator, CK-2127107, improves exercise tolerance in a rat model of heart failure. *J Pharmacol Exp Ther.* 2015;353:159–168.
- [2] Genet M, Lee LC, Baillargeon B, et al. Modeling pathologies of diastolic and systolic heart failure. *Ann Biomed Eng.* 2016;44:112–127.
- [3] Chaudhry SP, Stewart GC. New pharmacological and technological management strategies in heart failure. *Vasc Health Risk Manag.* 2017;13:111–121.
- [4] Hohl M, Wagner M, Reil JC, et al. HDAC4 controls histone methylation in response to elevated cardiac load. *J Clin Invest.* 2013;123:1359–1370.
- [5] Rossignol P, Hernandez AF, Solomon SD, et al. Heart failure drug treatment. *Lancet.* 2019;393:1034–1044.
- [6] Deng B, Wang JX, Hu XX, et al. Nkx2.5 enhances the efficacy of mesenchymal stem cells transplantation in treatment heart failure in rats. *Life Sci.* 2017;182:65–72.
- [7] Thorup L, Simonsen U, Grimm D, et al. Ivabradine: current and future treatment of heart failure. *Basic Clin Pharmacol Toxicol.* 2017;121:89–97.
- [8] Mano H. Epigenetic abnormalities in cardiac hypertrophy and heart failure. *Environ Health Prev Med.* 2008;13:25–29.
- [9] Lu J, Song G, Tang Q, et al. *IRX1* hypomethylation promotes osteosarcoma metastasis via induction of *CXCL14/NF-kappaB* signaling. *J Clin Invest.* 2015;125:1839–1856.
- [10] Movassagh M, Choy MK, Goddard M, et al. Differential DNA methylation correlates with differential expression of angiogenic factors in human heart failure. *PLoS One.* 2010;5:e8564.
- [11] Xiao D, Dasgupta C, Chen M, et al. Inhibition of DNA methylation reverses norepinephrine-induced cardiac hypertrophy in rats. *Cardiovasc Res.* 2014;101:373–382.
- [12] Liu X, Zhang J, Liu L, et al. Protein arginine methyltransferase 5-mediated epigenetic silencing of *IRX1* contributes to tumorigenicity and metastasis of gastric cancer. *Biochimica Et Biophysica Acta Molecular Basis of Disease.* 2018;1864:2835–2844.

- [13] Guo C, Wang Q, Wang Y, et al. Exome sequencing reveals novel IRXI mutation in congenital heart disease. *Mol Med Rep.* 2017;15:3193–3197.
- [14] Park SH, Kim SK, Choe JY, et al. Hypermethylation of EBF3 and IRX1 genes in synovial fibroblasts of patients with rheumatoid arthritis. *Mol Cells.* 2013;35:298–304.
- [15] Hromas R, Broxmeyer HE, Kim C, et al. Cloning of BRAK, a novel divergent CXC chemokine preferentially expressed in normal versus malignant cells. *Biochem Biophys Res Commun.* 1999;255:703–706.
- [16] Moser B, Loetscher P. Lymphocyte traffic control by chemokines. *Nat Immunol.* 2001;2:123–128.
- [17] Payne AS, Cornelius LA. The role of chemokines in melanoma tumor growth and metastasis. *J Invest Dermatol.* 2002;118:915–922.
- [18] Frederick MJ, Henderson Y, Xu X, et al. In vivo expression of the novel CXC chemokine BRAK in normal and cancerous human tissue. *Am J Pathol.* 2000;156:1937–1950.
- [19] Shurin GV, Ferris RL, Tourkova IL, et al. Loss of new chemokine CXCL14 in tumor tissue is associated with low infiltration by dendritic cells (DC), while restoration of human CXCL14 expression in tumor cells causes attraction of DC both in vitro and in vivo. *J Immunol.* 2005;174:5490–5498.
- [20] Shellenberger TD, Wang M, Gujrati M, et al. BRAK/CXCL14 is a potent inhibitor of angiogenesis and a chemotactic factor for immature dendritic cells. *Cancer Res.* 2004;64:8262–8270.
- [21] Schwarze SR, Luo J, Isaacs WB, et al. Modulation of CXCL14 (BRAK) expression in prostate cancer. *Prostate.* 2005;64:67–74.
- [22] Ozawa S, Kato Y, Komori R, et al. BRAK/CXCL14 expression suppresses tumor growth in vivo in human oral carcinoma cells. *Biochem Biophys Res Commun.* 2006;348:406–412.
- [23] Wentz MN, Mayer C, Gaida MM, et al. CXCL14 expression and potential function in pancreatic cancer. *Cancer Lett.* 2008;259:209–217.
- [24] Tian Y, Morris TJ, Webster AP, et al. ChAMP: updated methylation analysis pipeline for Illumina BeadChips. *Bioinformatics.* 2017;33:3982–3984.
- [25] Zhou Y, Shiok TC, Richards AM, et al. MicroRNA-101a suppresses fibrotic programming in isolated cardiac fibroblasts and in vivo fibrosis following trans-aortic constriction. *J Mol Cell Cardiol.* 2018;121:266–276.
- [26] Kaimoto S, Hoshino A, Ariyoshi M, et al. Activation of PPAR-alpha in the early stage of heart failure maintained myocardial function and energetics in pressure-overload heart failure. *Am J Physiol Heart Circ Physiol.* 2017;312:H305–H313.
- [27] Lee PJ, Rudenko D, Kuliszewski MA, et al. Survivin gene therapy attenuates left ventricular systolic dysfunction in doxorubicin cardiomyopathy by reducing apoptosis and fibrosis. *Cardiovasc Res.* 2014;101:423–433.
- [28] Huang CY, Kuo WW, Lo JF, et al. Doxorubicin attenuates CHIP-guarded HSF1 nuclear translocation and protein stability to trigger IGF-IIR-dependent cardiomyocyte death. *Cell Death Dis.* 2016;7:e2455.
- [29] Mayer SC, Gilsbach R, Preissl S, et al. Adrenergic repression of the epigenetic reader MeCP2 facilitates cardiac adaptation in chronic heart failure. *Circ Res.* 2015;117:622–633.
- [30] Jeong D, Lee MA, Li Y, et al. Matricellular protein CCN5 reverses established cardiac fibrosis. *J Am Coll Cardiol.* 2016;67:1556–1568.
- [31] Leach JP, Heallen T, Zhang M, et al. Hippo pathway deficiency reverses systolic heart failure after infarction. *Nature.* 2017;550:260–264.
- [32] Li LC, Dahiya R. MethPrimer: designing primers for methylation PCRs. *Bioinformatics.* 2002;18:1427–1431.
- [33] Wassenaar JW, Gaetani R, Garcia JJ, et al. Evidence for mechanisms underlying the functional benefits of a myocardial matrix hydrogel for post-MI treatment. *J Am Coll Cardiol.* 2016;67:1074–1086.
- [34] Sun X, Sui Q, Zhang C, et al. Targeting blockage of STAT3 in hepatocellular carcinoma cells augments NK cell functions via reverse hepatocellular carcinoma-induced immune suppression. *Mol Cancer Ther.* 2013;12:2885–2896.
- [35] Jones PA. Functions of DNA methylation: islands, start sites, gene bodies and beyond. *Nat Rev Genet.* 2012;13:484–492.
- [36] Chatterjee A, Rodger EJ, Morison IM, et al. Tools and strategies for analysis of genome-wide and gene-specific DNA methylation patterns. *Methods Mol Biol.* 2017;1537:249–277.
- [37] Reuter JA, Spacek DV, Snyder MP. High-throughput sequencing technologies. *Mol Cell.* 2015;58:586–597.
- [38] Ribas L, Vanezis K, Imues MA, et al. Treatment with a DNA methyltransferase inhibitor feminizes zebrafish and induces long-term expression changes in the gonads. *Epigenetics Chromatin.* 2017;10:59.
- [39] Liu LC, Damman K, Lipsic E, et al. Heart failure highlights in 2012–2013. *Eur J Heart Fail.* 2014;16:122–132.
- [40] He W, Jia Y, Takimoto K. Interaction between transcription factors Iroquois proteins 4 and 5 controls cardiac potassium channel Kv4.2 gene transcription. *Cardiovasc Res.* 2009;81:64–71.
- [41] Asaka S, Fujimoto T, Akaishi J, et al. Genetic prognostic index influences patient outcome for node-positive breast cancer. *Surg Today.* 2006;36:793–801.
- [42] Houweling AC, Dildrop R, Peters T, et al. Gene and cluster-specific expression of the Iroquois family members during mouse development. *Mech Dev.* 2001;107:169–174.
- [43] Blenck CL, Harvey PA, Reckelhoff JF, et al. The importance of biological sex and estrogen in rodent models of cardiovascular health and disease. *Circ Res.* 2016;118:1294–1312.
- [44] Kianmehr M, Ghorani V, Boskabady MH. Animal model of asthma, various methods and measured

- parameters: A methodological review. *Iran J Allergy Asthma Immunol.* [2016](#);15:445–465.
- [45] Schaefer A, Schneeberger Y, Stenzig J, et al. A new animal model for investigation of mechanical unloading in hypertrophic and failing hearts: combination of transverse aortic constriction and heterotopic heart transplantation. *PLoS One.* [2016](#);11:e0148259.
- [46] Breckenridge R. Heart failure and mouse models. *Dis Model Mech.* [2010](#);3:138–143.
- [47] Piek A, de Boer RA, Sillje HH. The fibrosis-cell death axis in heart failure. *Heart Fail Rev.* [2016](#);21:199–211.
- [48] Santiago JJ, McNaughton LJ, Koleini N, et al. High molecular weight fibroblast growth factor-2 in the human heart is a potential target for prevention of cardiac remodeling. *PLoS One.* [2014](#);9:e97281.
- [49] Hu Y, Li L, Shen L, et al. FGF-16 protects against adverse cardiac remodeling in the infarct diabetic heart. *Am J Transl Res.* [2017](#);9:1630–1640.